

# Neutrino/antineutrino- $^{12}\text{C}$ charged cross sections in the projected QRPA formalism

A. R. Samana, C. A. Bertulani

*Department of Physics, Texas A&M University Commerce, P.O.3011 Commerce, 75429 TX, USA*

and F. Krmpotić<sup>1,2,3</sup>

<sup>1</sup>*Instituto de Física La Plata, CONICET, 1900 La Plata, Argentina*

<sup>2</sup>*Facultad de Ciencias Astronómicas y Geofísicas,*

*Universidad Nacional de La Plata, 1900 La Plata, Argentina, and*

<sup>3</sup>*Departamento de Física, Universidad Nacional de La Plata, C. C. 67, 1900 La Plata, Argentina*

(Dated: October 27, 2018)

The  $\nu/\bar{\nu}$ - $^{12}\text{C}$  cross sections are evaluated in the projected quasiparticle random phase approximation (PQRPA). The cross section for  $\nu_e$  as a function of the incident neutrino energy is compared with recent theoretical calculations of more sophisticated models. The  $\bar{\nu}$ - $^{12}\text{C}$  cross section is calculated for the first time with the PQRPA. The distribution of cross sections averaged with the Michel spectrum as well as with other estimated fluxes for future experiments is compared for both  $\nu_e$  and  $\bar{\nu}_e$ . Some astrophysical implications are addressed.

PACS numbers: 23.40.-s, 25.30.Pt, 26.50.+x

## I. INTRODUCTION

Among the different semileptonic weak interaction with nuclei, such as charged lepton capture and  $\beta^\pm$ -decays, the neutrino (antineutrino) scattering is one of most promising tools for studies of physics beyond the standard model. The massiveness of neutrinos and the related oscillation are strongly sustained by many experiment works involving atmospheric, solar, reactor and accelerator neutrinos [1, 2, 3, 4, 5, 6, 7]. Processes such as  $\beta$ -decay, electron capture and the double beta decay with two neutrinos are employed to constraint predictions on neutrinoless double beta decay [8]. Because the neutrinos interact so weakly with matter, they are used as messengers from stars and give us useful information on the possible dynamics of supernova collapse and explosion as well as on the synthesis of heavy nuclei [9, 10, 11]. On the other hand, Lazauskas *et al.* have shown in Ref. [12] that neutrino-nucleus cross interactions can explore the possibility of performing nuclear structure studies using low-energy neutrino beams.

The neutrino-nucleus scattering formalism was developed in several references. For example, the pioneer work of O'Connell *et al.* [13, 14] describes all semileptonic processes, whereas Kuramotos's formalism [15] only explains the neutrino-nucleus cross section and additional framework is necessary for the muon capture rates Ref.[16]. Krmpotić *et al.* have shown in Ref. [17] that all these formalisms are equivalent because they can be described with the same nuclear matrix elements derived from an effective hamiltonian obtained by carrying out the Foldy-Wouthuysen transformation and retaining terms up to order  $\mathcal{O}(\mathbf{k}/M)$ , where  $\mathbf{k}$  is the momentum transfer and  $M$  is the nucleon mass.

The neutrino-nucleus scattering on  $^{12}\text{C}$  is important because this nucleus is a component in many liquid scintillator detectors. Experiments such as KARMEN [18, 19], LAMPF [20, 21] and LSND [1, 2] have used  $^{12}\text{C}$  to

search for neutrino oscillations and to measure neutrino-nucleus cross sections. As the  $^{12}\text{C}$  nucleus forms one of the onion-like shells of a large star before collapse, it is also important for astrophysics studies. Future experiments are planning to use  $^{12}\text{C}$  as liquid scintillator, such as in the spallation neutron source (SNS) at Oak Ridge National Laboratory (ORNL) [22], or in the LVD (Large Volume Detector) experiment [23], developed in the INFN Gran Sasso in Italy.

There have been great efforts on nuclear structure models to describe consistently semileptonic weak processes with  $^{12}\text{C}$  such as RPA-like models: RPA [24, 25, 26], CRPA [27, 28, 29], QRPA[24, 30], PQRPA[17, 30], relativistic QRPA (RQRPA) [31]; Local Fermi Gas (LFG) plus RPA [32, 33], phenomenological models [34, 35, 36, 37] and the well known SM [24, 38, 39]. Figure 1 summarizes the state of the art of the most recent electron and muon neutrinos cross section on  $^{12}\text{C}$  as function of the neutrino energy for several nuclear structure calculations. The residual interaction used in those calculations is not unique and it varies from the simple  $\delta$ -interaction in PQRPA [17], Skyrme-type effective interaction in QRPA- SM- RPA [24], G matrix for the Boon (or Landau Migdal) potential in CRPA [28], meson-exchange density dependent relativistic mean field effective interactions - DD-ME2 and finite range Gogny interaction in RQRPA [31], and nucleon-nucleon effective force supplemented by nucleon- $\Delta(1232)$  and  $\Delta(1232)$ - $\Delta(1232)$  interactions in LFG+RPA [32]. From Figure 1 we note that the behavior of  $\sigma$  from both  $\nu_e$ - $^{12}\text{C}$  and  $\nu_\mu$ - $^{12}\text{C}$  reactions evaluated in SM, RPA and PQRPA diverges substantially from CRPA and LFG+RPA with increasing neutrino energy. One sees that, while within the SM and the PQRPA both  $\sigma_\ell$  ( $\ell = e, \mu$ ) start to level at around 200 MeV, the RPA does the same but around 300 MeV. The CRPA and LFG+RPA are those models where the cross sections continue to increase at these energies. It should be pointed out, however, that all three RPA-like

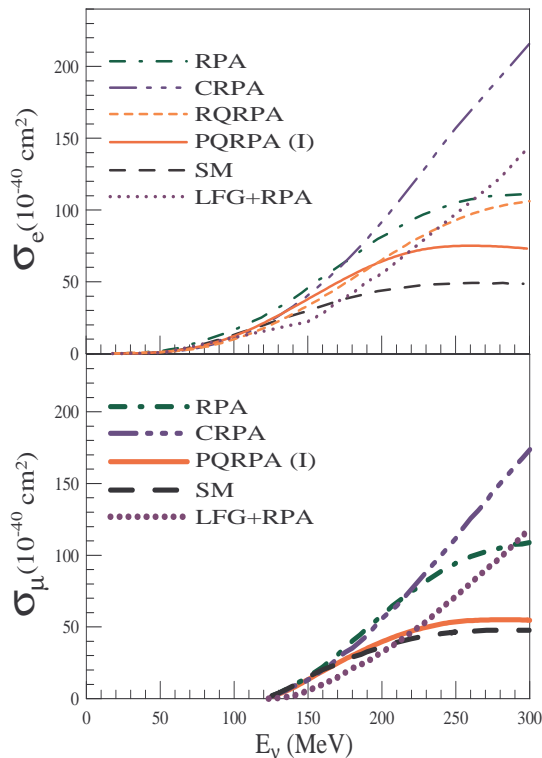


FIG. 1: (Color online) Comparison of the  $\sigma_{e,\mu}(E_\nu)$  (top panel) and  $\sigma_\mu(E_\nu)$  (bottom panel) as function of  $\nu_e$  and  $\nu_\mu$  neutrino incident energy for different nuclear structure models CRPA [28] (dashed-dot-dot), PQRPA [17] (solid), RPA [24] (dashed-dot), SM [24] (long dashed), LFG+RPA [32] (dot) and RQRPA [31] (short dashed).

calculations used the same single-particle space and only 1p-1h (2 quasiparticles) excitations have been considered. The major differences comes from the type of correlations included in each case. In Ref. [17] it was noted that the similarity between the SM and the PQRPA results, as well as the difference with the RPA calculations, can be attributed to the Pauli Principle. But, it is hard to understand the qualitative difference between the RPA and CRPA. It could happen that some additional effects, such as contributions of high-lying single-particle states or of 2p-2h (4 quasiparticles) excitations, become important for neutrino energies above the DIF energy region, preventing in this way the leveling of  $\sigma(E_\nu)$ . This is an important issue and worth to be analyzed, in particular in view of the recent LFG+RPA results in the QE (quasi-elastic) region at intermediate energies, where  $\sigma$  becomes flat only at about 1 GeV. This is an open question that should be considered in future studies.

Refs. [17, 30, 40] have shown that in order to describe the weak decay observables in a light  $N = Z$  nucleus as such as  $^{12}\text{C}$  in the framework of the RPA model one must, besides including the BCS correlations, also include the particle number projection procedure. Recently in Ref. [41], the PQRPA was used to calculate the  $^{56}\text{Fe}(\nu_e, e^-)^{56}\text{Co}$  cross section. The resulting cross sec-

tion was compared with a QRPA calculation with the same interaction showing that the projection procedure is important for medium mass nuclei. In heavy nuclei, where the neutron excess is usually large, the projection procedure is less important [42].

In this work the neutrino and antineutrino-nucleus  $\sigma(E_\nu)$  cross section are evaluated with the formalism developed in Ref. [17] for neutrino-nucleus reactions using the PQRPA as the nuclear structure model. We adopt that formalism because it is best suited for a nuclear structure comparison. With a minor modification on this formalism in the leptonic traces, we evaluate the antineutrino reactions. As the PQRPA model solves the inconveniences that appear in applying RPA-like models to describe the nuclear structure of the  $\{^{12}\text{B}, ^{12}\text{C}, ^{12}\text{N}\}$  triad, we calculate the  $^{12}\text{C}(\bar{\nu}_e, e^+)^{12}\text{B}$  cross section with the nuclear matrix elements (NME) in this model.

It was shown in [30] that large multipoles are important in the detection window  $E_e \in [60 - 200]$  MeV of LSND for  $\nu_\mu \rightarrow \nu_e$  neutrino oscillations. This yields an enhancement of the  $\nu_\mu \rightarrow \nu_e$  oscillation probability. Recent results of  $\sigma(E_\nu)$  for different multipoles with RQRPA [31] allow us to compare with those provided by PQRPA. For the sake of completeness the partial contribution to the inclusive cross section for  $\bar{\nu}_e - ^{12}\text{C}$  is analyzed. One alternative method to study the large multipoles was discussed by Lazauskus and Volpe in Ref. [12] through the so called low-energy neutrino beta-beams. Different distributions of the averaged cross sections on nuclei as  $^{16}\text{O}$ ,  $^{16}\text{Fe}$ ,  $^{100}\text{Mo}$ , and  $^{208}\text{Pb}$  were presented and the feasibility of using beta-beams was clarified. With that work we have learned that low-energy neutrino beams could provide information on the forbidden states, in particular the spin-dipole. The QRPA model was employed to describe nuclei beyond the closed-shell approximation. However, QRPA predictions of Ref. [24] do not yield good results for  $^{12}\text{C}$  because the configuration mixing is not properly accounted for and the projection procedure (as done in Ref. [17]) is not included. We have mentioned previously that  $^{12}\text{C}$  is reasonably well described with the PQRPA and so, we can expand the discussion of the  $\beta$ -beam to this nucleus. In spite of this fact we fold the cross section with the DAR flux and those from beta-beams and compare these results. Some topics on astrophysical applications with the resulting cross sections are addressed.

In Sec. II we briefly overview the formalism for the neutrino-nucleus cross sections as well the PQRPA. In Sec. III we compare the  $\nu/\bar{\nu} - ^{12}\text{C}$  cross sections with other RPA-like models. Summarizing conclusion are presented in Sec. IV.

## II. FORMALISM NEUTRINO-NUCLEUS

The cross section for  $\nu_e + (Z, A) \rightarrow (Z+1, A) + e^-$ , as a function of the incident neutrino energy for each nuclear

spin, is given by

$$\sigma(E_e, J_f) = \frac{|\mathbf{p}_e|E_e}{2\pi} F(Z+1, E_e) \int_{-1}^1 d(\cos\theta) \mathcal{T}_\sigma(|\mathbf{k}|, J_f), \quad (1)$$

where  $F(Z+1, E_e)$  is the usual scattering Fermi function,  $k = p_e - q_\nu$  is the momentum transfer,  $p_e$  and  $q_\nu$  are the corresponding electron and neutrino momenta, and  $\theta \equiv \hat{\mathbf{q}}_\nu \cdot \hat{\mathbf{p}}_e$  is the angle between the incident neutrino and emerging electron. The  $\sigma(E_e, J_f)$  cross sections are obtained within first-order perturbation theory according to Ref. [17], where velocity-dependent terms are included in the weak effective Hamiltonian. The transition amplitude  $\mathcal{T}_\sigma(|\mathbf{k}|, J_f)$  depends on the neutrino leptonic traces and on the nuclear matrix elements (NME), as explained in Ref. [17]. They are evaluated in the PQRPA.

In Refs. [17, 40, 41] we evaluated the neutrino-nucleus reaction  $\nu_e + (Z, A) \rightarrow (Z+1, A) + e^-$  for  $^{12}\text{C}$ . To evaluate the antineutrino-nucleus reaction  $\bar{\nu}_e + (Z, A) \rightarrow (Z-1, A) + e^+$  with this formalism it is necessary to modify the lepton trace  $\mathbf{L}_{\pm 1, \pm 1}$ , that appears in [17, (2.35)], to

$$\mathbf{L}_{\pm 1, \pm 1} = 1 - \frac{q_0 p_0}{E_\ell E_\nu} \pm \left( \frac{q_0}{E_\nu} - \frac{p_0}{E_\ell} \right) S_1, \quad (2)$$

where the factor  $S_1 = \pm 1$  for neutrino/antineutrino reactions. The inclusive  $(\nu/\bar{\nu})$ -nucleus cross section reads

$$\sigma_\ell^{\text{inc}}(E_\nu) = \sum_{J_f^\mp} \sigma_\ell(E_\ell = E_\nu - \omega_{J_f^\mp}, J_f^\mp); \quad \ell = \begin{cases} e, & \text{for } e^-, \\ \bar{e}, & \text{for } e^+. \end{cases} \quad (3)$$

The spin and parity dependent cross section  $\sigma_\ell(E_\ell, J_f^\mp)$  is given by equation (1) (explicitly by [17, (2.19)]) with the additional modification (2);  $\omega_{J_f^\mp}$  are the excitation energies for each nuclear state in the daughter nuclei  $(A, N \pm 1)$  (the '+' for neutrino-nucleus reaction and the '-' for antineutrino one) relative to the ground state in the parent nuclei  $(A, N)$ .

The flux averaged cross section reads

$$\bar{\sigma}_\ell = \int dE_\nu \sigma_\ell(E_\nu) n_\ell(E_\nu), \quad (4)$$

where  $\sigma_e(E_\nu)$  ( $\sigma_{\bar{e}}(E_\nu)$ ), is the neutrino (antineutrino) cross section as a function of the neutrino (antineutrino) energy eq. (3) and  $n_\ell(E_\nu)$  is the neutrino (antineutrino) normalized flux. In Refs. [17, 40] we have folded the  $\sigma_e(E_\nu)$  with the Michel energy spectrum [19, 43]

$$n_e(E_\nu) = \frac{96E_\nu^2}{M_\mu^4} (M_\mu - 2E_\nu),$$

where  $M_\mu$  is the muon mass, in . This neutrino flux is normalized to one in the DAR (decay-at-rest) energy interval. In this work, we fold the antineutrino cross section,  $\sigma_{\bar{e}}(E_\nu)$ , with antineutrino fluxes from conventional DAR source [19], and with those from the decay

of  $^6\text{He}$  ions boosted at  $\gamma = 6$ ,  $\gamma = 10$ , and  $\gamma = 14$  presented in Fig. 4 of Ref. [12]. Specific details on the neutrino fluxes associated to low-energy  $\beta$ -beams are given in Refs. [12, 44].

The formalism of the PQRPA was developed in Refs. [17, 42]. When the excited states  $|J_f\rangle$  in the final  $(Z \pm 1, N \mp 1)$  nuclei are described within the PQRPA, the transition amplitudes for the multipole charge-exchange operator  $\mathbf{Y}_J$ , read

$$\begin{aligned} \langle J_f, Z + \mu, N - \mu | \mathbf{Y}_J | 0^+ \rangle &= \frac{1}{(IZIN)^{1/2}} \\ \sum_{pn} \left[ \frac{\Lambda_\mu(pnJ)}{(IZ^{-1+\mu}(p)I^{N-1+\mu}(n))^{1/2}} X_\mu^*(pnJ_f) + \right. \\ &\left. + \frac{\Lambda_{-\mu}(pnJ)}{(IZ^{-1-\mu}(p)I^{N-1-\mu}(n))^{1/2}} Y_\mu^*(pnJ_f) \right], \quad (5) \end{aligned}$$

with the one-body matrix elements given by

$$\Lambda_\mu(pnJ) = -\frac{\langle p | \mathbf{Y}_J | n \rangle}{\sqrt{2J+1}} \begin{cases} u_p v_n, & \text{for } \mu = +1 \\ u_n v_p, & \text{for } \mu = -1 \end{cases}, \quad (6)$$

where

$$\begin{aligned} I^K(k_1 k_2 \cdots k_n) &= \frac{1}{2\pi i} \oint \frac{dz}{z^{K+1}} \sigma_{k_1} \cdots \sigma_{k_n} \\ &\times \prod_k (u_k^2 + z^2 v_k^2)^{j_k+1/2}; \\ \sigma_k^{-1} &= u_k^2 + z^2 v_k^2, \quad (7) \end{aligned}$$

are the PBCS number projection integrals, and  $(u_k, v_k)$  are the usual occupation amplitudes of the  $k$ -level. The forward,  $X_\mu$ , and backward,  $Y_\mu$ , PQRPA amplitudes are obtained by solving the RPA equations, as explained in Ref. [17]. It is possible to recover the usual QRPA from the PQRPA dropping the index  $\mu$  in the RPA matrixes and taking the limit  $I^K \rightarrow 1$ , and substituting the unperturbed PBCS energies by the BCS energies relative to the Fermi level. It is also necessary to impose the subsidiary conditions  $Z = \sum_{j_p} (2j_p + 1)^2 v_{j_p}^2$  and  $N = \sum_{j_n} (2j_n + 1)^2 v_{j_n}^2$  to average the number of particles because they are no longer good quantum numbers.

### III. NUMERICAL RESULTS AND DISCUSSION

In this section, our theoretical results for the cross section  $\nu_e + ^{12}\text{C} \rightarrow ^{12}\text{N} + e^-$  and  $\bar{\nu}_e + ^{12}\text{C} \rightarrow ^{12}\text{B} + e^+$  within the PQRPA are compared with other RPA-type model. As with our previous work [41], we employ the  $\delta$ -interaction (in  $\text{MeV fm}^3$ )

$$V = -4\pi (v_s P_s + v_t P_t) \delta(r),$$

with different coupling constants  $v_s$  and  $v_t$  for the particle-hole, particle-particle, and pairing channels. This interaction leads to a good description of single and double  $\beta$ -decays and it has been used extensively

in the literature [45, 46, 47, 48]. The configuration space includes the single-particle orbitals with  $nl = (1s, 1p, 1d, 2s, 1f, 2p)$  for both protons and neutrons. The s.p. energies, pairing strengths and projection procedure are detailed in Tables III and VI of Ref. [17]. The single-particle wave functions were also approximated with those of the HO with the length parameter  $b = 1.67\text{fm}$ , which corresponds to  $\hbar\omega = 45A^{-1/3} - 25A^{-2/3}$  MeV for the oscillator energy. In our previous works Refs. [17, 40] we have also pointed out that the values of the coupling strengths  $v_s$  and  $v_t$  within the  $pp$  and  $ph$  channels used in  $N > Z$  nuclei ( $v_s^{pp} \equiv v_s^{pair}$ , and  $v_t^{pp} \gtrsim v_s^{pp}$ ), might not be suitable for  $N = Z$  nuclei. Then, the best agreement with data in  $^{12}\text{C}$  (energy of the ground state in  $^{12}\text{C}$ ,  $B(GT)$  of  $^{12}\text{N}(\beta^+)^{12}\text{C}$ , and exclusive muon capture on  $^{12}\text{B} \equiv \lambda^{exc}(1_1^+)$ ) is obtained when the  $pp$  channel is totally switched off, *i.e.*,  $v_s^{pp} \equiv v_t^{pp} = 0$ . Three different set of values for the  $ph$  coupling strengths with physical meaning are [40]: P(I):  $v_s^{ph} = v_s^{pair} = 24$  MeV fm<sup>3</sup> and  $v_t^{ph} = v_s^{ph}/0.6 = 39.86$  MeV fm<sup>3</sup>; P (II):  $v_s^{ph} = 27$  MeV fm<sup>3</sup> and  $v_t^{ph} = 64$  MeV fm<sup>3</sup>; and P (III):  $v_s^{ph} = v_t^{ph} = 45$  MeV fm<sup>3</sup>.

Among the different models that studied the observables in the  $\{^{12}\text{B}, ^{12}\text{C}, ^{12}\text{N}\}$  triad, some countable examples give an estimate of the systematic error on the cross section as a whole, *i.e.*, based on the measured observables in the triad. The LSND experiment [2] has used the CRPA cross section with systematic uncertainties of (+22%, -45%) folded with the muon neutrino fluxes. When the PQRPA was used to reanalyze the LSND data for the  $\nu_\mu \rightarrow \nu_e$  oscillation search, an uncertainty on the folded cross section was  $\pm 28\%$ , where only  $\approx 20\%$  was based on theoretical uncertainties. Here, we do not pretend to make a detailed study of the uncertainties of the model such as that developed by Valverde *et al.* in Ref. [33] for the LFG+RPA model, instead we are going to establish a simple criteria of uncertainty for the parametrization of residual  $\delta$ -interaction in the PQRPA using the experimental data available on the literature. Table I shows a summary of the weak observables as described in the PQRPA model for  $\{^{12}\text{B}, ^{12}\text{C}, ^{12}\text{N}\}$  triad in previous References [17, 40]. As a measure of how good is the parametrization employed in this model, we define the parameters of deviation from the experimental values as

$$\eta = \sqrt{\frac{1}{N_0} \sum_{n=1}^{N_0} \left( \frac{y_{cal}(n) - y_{exp}(n)}{\delta y_{exp}(n)} \right)^2},$$

$$\bar{\epsilon} = \left[ \sum_{n=1}^{N_0} \left( \frac{y_{cal}(n) - y_{exp}(n)}{y_{exp}(n)} \right) \right] \frac{100\%}{N_0}. \quad (8)$$

These parameters were evaluated with the observables of Table I,  $y_{cal/exp}(n) \equiv \{\lambda^{exc}(1_1^+), \dots, B(GT)\}$ , with  $N_0 = 10$  for  $\eta_A$ , and  $N_0 = 9$  for  $\eta_B$  where  $E_{gs}(^{12}\text{N})$  is excluded. From the  $\eta_A$  values we note that the P(I) parametrization achieves the lower value if we conserve

TABLE I: Weak observables reproduced in the PQRPA model for the  $\{^{12}\text{B}, ^{12}\text{C}, ^{12}\text{N}\}$  triad in comparison with the experimental values. In the last three lines, we show the deviation parameters  $\eta_A, \eta_B$  and  $\bar{\epsilon}$  (in %) described in the text. The  $B(GT)$  is the averaged value for  $B(GT_+)$  and  $B(GT_-)$ . The  $\lambda$ -values are in units of  $10^3 \text{ s}^{-1}$ ,  $\bar{\sigma}_e$  and  $\bar{\sigma}_\mu$ -values in units of  $10^{-42} \text{ cm}^2$  and  $10^{-40} \text{ cm}^2$  respectively,  $E_{gs}(^{12}\text{N})$  is in MeV and  $B(GT)$  is dimensionless.

Obs.	P(I)	P(II)	P(III)	Exp
$\lambda^{exc}(1_1^+)$	7.52	6.27	6.27	$6.2 \pm 0.3$ [49]
$\lambda(1_1^-)$	1.06	0.49	0.98	$0.62 \pm 0.2$ [50, 51]
$\lambda(2_1^-)$	0.31	0.18	0.16	$0.18 \pm 0.1$ [50, 51]
$\lambda^{inc}$	48.16	42.56	44.67	$38 \pm 1$ [52]
$\bar{\sigma}_e^{exc}$	9.94	8.07	8.17	$8.9 \pm 0.9$ [53]
$\bar{\sigma}_e^{inc}$	21.67	18.6	17.54	$13.2 \pm 0.7$ [53]
$\bar{\sigma}_\mu^{exc}$	0.74	0.59	0.59	$0.56 \pm 0.13$ [54]
$\bar{\sigma}_\mu^{inc}$	14.69	12.94	13.51	$10.6 \pm 1.8$ [54]
$E_{gs}(^{12}\text{N})$	17.89	18.14	18.13	$17.3381 \pm 0.001$ [55]
$B(GT)$	0.568	0.477	0.48	$0.496 \pm 0.030$ [56]
$\eta_A$	175	253	250	
$\eta_B$	5.7	3.0	3.1	
$\bar{\epsilon}$ (%)	35	12	17	

the  $E_{gs}(^{12}\text{N})$ . For  $\eta_B$  values of P(II) and P(III) we noted that they are of the same order and that the deviation in the ground state energy increases the partial contribution in the sum due to its lower experimental error. We can conclude from the values of  $\bar{\epsilon}$  that the PQRPA results overestimate in  $\approx 21\%$  the experimental values. We remark that the parameters of the residual interaction,  $v_T^{PP}$  (in  $pp$  channel) and  $v_s^{PH}$  (in  $ph$  channel), were fixed to reproduce only the  $E_{gs}(^{12}\text{N})$  and  $B(GT)$ , whereas the other obtained observables are predictions of our model. In this way, we estimate and analyze the antineutrino cross section with P(I). Their results are considered as a upper limit for PQRPA. The P(II) results are better estimates for this model.

Let us summarize some interesting issues for the exclusive cross section,  $\sigma^{exc}$ , that involves only the transitions to the ground state, in the view of some future experiments that will use  $^{12}\text{C}$  as scintillator liquid detector to search signals of supernovae neutrinos. In the LVD experiment [23] it was estimated that the  $(\nu_e + \bar{\nu}_e)$  interactions on  $^{12}\text{C}$  affect the total detected signal. The LVD detector use exclusive cross sections, *i.e.*,  $^{12}\text{C}_{gs}(O^+)(\nu_e, e^-)^{12}\text{B}_{gs}(1^+)$  and  $^{12}\text{C}_{gs}(0^+)(\bar{\nu}_e, e^+)^{12}\text{B}_{gs}(1^+)$ , from the EPT (Elementary Particle Treatment) model [34] to compare with the expected signal in the detector. This theoretical description of exclusive cross section was used for estimate possible events of supernovae neutrinos in experiments like Borexino [57] and LENA [58]. In all the different variation on the parameters studied by the LVD group, the cross section was kept fixed within error. It could be reasonable for the exclusive neutrino cross section  $^{12}\text{C}$ , that is theo-

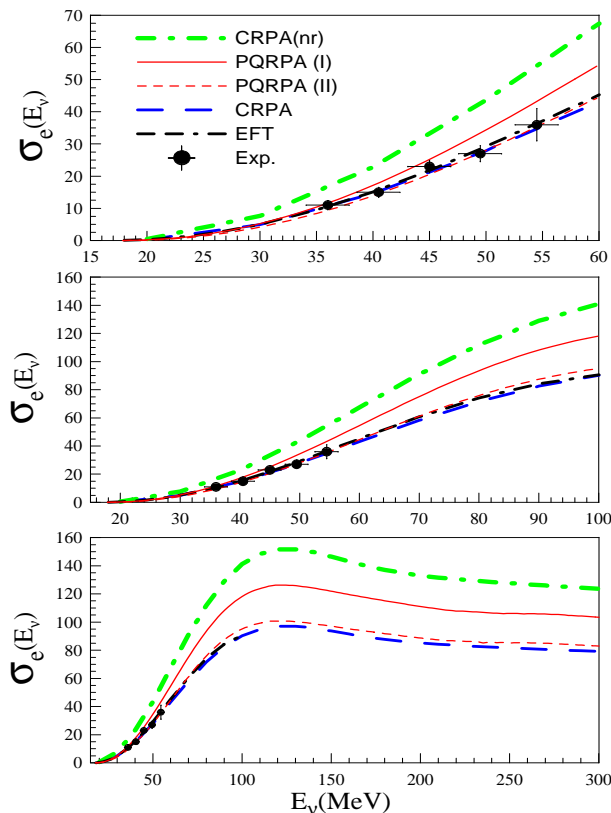


FIG. 2: (Color online) Exclusive  $\nu_e - {}^{12}\text{C}$  cross section in different nuclear structure models, CRPA and CRPA(nr) [27], PQRPA [30] and EPT [34]. In the top panel theoretical cross sections are compared with the experimental data of Ref. [39] in the DAR region. The middle and bottom panels show the cross sections for other energy intervals, as described in the text.

retically and experimentally well determined. The exclusive folded cross section for  $(\nu_e, {}^{12}\text{C})$   $\bar{\sigma}_e^{\text{exc}} \equiv \bar{\sigma}_e(J_f^\pi = 1_1^+)$  was measured by LAMPF [20, 21], KARMEN Collaboration [18] and LSND Collaboration [1, 2] in the DAR region. In general, theoretical estimates for  $\bar{\sigma}_e^{\text{exc}}$  are in agreement with the experimental data. For this reason, this cross section was used to calibrate different experiments leaving a faithful knowledge of neutrino fluxes in order to search neutrino oscillations [3, 19]. It was also employed to demonstrate the feasibility of observing low-energy neutrino induced transitions between well determined nuclear states.

Figure 2 shows the  $\sigma_e(J_f^\pi = 1_{gs}^+)$  as function of the incident neutrino energy for PQRPA [30], CRPA [27] and EPT [34] on the energy interval important for search of neutrino oscillations (top panel), for supernovae neutrinos (middle panel), and to the upper limit of 300 MeV (bottom panel). CRPA used a reduction factor average of  $\approx 1.5$  to reproduce the  $B(GT)$  of  ${}^{12}\text{N}(\beta^+){}^{12}\text{C}$  and  ${}^{12}\text{B}(\beta^-){}^{12}\text{C}$  together with the exclusive muon capture in  ${}^{12}\text{B} \equiv \lambda^{\text{exc}}(1_1^+)$ . This factor ensures that CRPA cross section is between the experimental error. CRPA (nr) non-reduced means that the CRPA cross section is mul-

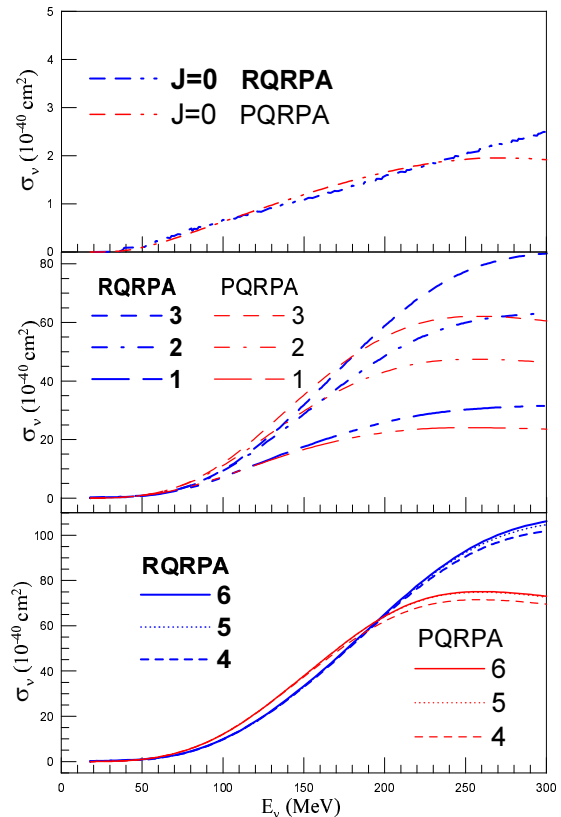


FIG. 3: (Color online) Comparison of the  $\sigma_e(E_\nu)$  in PQRPA and RQRPA [31] models for different multipoles showed according the increase nuclear spin from  $J_{min} = 0^\pm$  to  $J_{max} = 6^\pm$ .

tiplied by 1.5. The PQRPA reproduces the cross sections without need of a reduction factor. P(I) overestimates the experimental data over 45 MeV and P(II) is as good as the CRPA reduced and EPT [34]. Nevertheless, there is no need for a reduction factor with the large multipoles. The neutrino inclusive cross section with and without reduction factors does not present differences when the energy increases. In the middle panel of Figure 2 we shown  $\sigma(1_1^+)$  in the energy interval that will search for supernovae neutrinos. We note that the P(II), EPT and CRPA results are close in the DAR region. From 60 MeV to 100 MeV and up to 300 MeV they separate progressively with increasing neutrino energy.

Figure 3 compares the RQRPA [31] and PQRPA neutrino cross sections as a function of the neutrino energy according the increase nuclear spin from  $J_{min} = 0^\pm$  to  $J_{max} = 6^\pm$ , *i.e.*,

$$\begin{aligned}
 J = 0 &\equiv \sigma_e(0^+) + \sigma_e(0^-), \\
 J = 1 &\equiv \sigma_e(0^+) + \sigma_e(0^-) + \sigma_e(1^+) + \sigma_e(1^-), \\
 &\vdots \\
 &J_f^\pi = 6^+, 6^- \\
 J = 6 &\equiv \sum_{J_f^\pi = 0^+, 0^-} \sigma_e(J_f^\pi), \quad (9)
 \end{aligned}$$

in the same way as in Ref. [31]. Our PQRPA results

are similar to those obtained from the RQRPA. The largest contribution comes from  $J = 1^\pm$  and  $J = 2^\pm$  and the contribution of higher multiplicities gradually decreases. In other words they are due to the allowed  $\sigma_e(0^+, 1^+)$ , first forbidden  $\sigma_e(0^-, 1^-, 2^-)$ , second forbidden  $\sigma_e(2^+, 3^+)$ , third forbidden  $\sigma_e(3^-, 4^-)$ , fourth forbidden  $\sigma_e(4^+, 5^+)$  transitions (hereafter allowed transitions (AT) and forbidden transitions (FT)), where the contribution from the higher forbiddenness is decreasing gradually. In particular for  $J = 0$  and  $J = 1$  both models have similar cross section up to  $\approx 150$  MeV. With increasing  $J$  the differences in these models increase starting from lower neutrino energies. From the bottom panel of Fig. 2 we see that the inclusive cross sections  $J = 6$  begin to level out at 200 MeV for PQRPA and 300 MeV for RQRPA. Comparing the inclusive folded cross section in DAR region we have  $18.6 \times 10^{-42}$  cm<sup>2</sup> in PQRPA (II) and  $12.14 \times 10^{-42}$  cm<sup>2</sup> for RQRPA. We note that RQRPA is close to the experimental value  $13.2 \pm 0.7 \times 10^{-42}$  cm<sup>2</sup> [53]. But the situation is inverted for the DIF region for  $(\nu_\mu, \mu^-)$ , where the  $\bar{\sigma}_\mu^{\text{inc}}$  is  $12.9 \times 10^{-40}$  cm<sup>2</sup> in PQRPA (PII) and  $19.59 \times 10^{-40}$  cm<sup>2</sup> for RQRPA, *i.e.*, the PQRPA is closer to the experimental value  $12.4 \pm 0.7 \times 10^{-40}$  cm<sup>2</sup> [53]. In tables VI and VII of [17] the cross sections  $\bar{\sigma}_{e,\mu}(J_f^\pi)$  for each final state with spin and parity  $J_f^\pi$ , as well as the exclusive,  $\bar{\sigma}_{e,\mu}^{\text{exc}} \equiv \bar{\sigma}_{e,\mu}(J_f^\pi = 1_1^+)$ , and inclusive  $\bar{\sigma}_{e,\mu}^{\text{inc}} = \sum_{J_f^\pi} \bar{\sigma}_e(J_f^\pi)$  are presented. It should be remembered that the main contribution to  $\bar{\sigma}_e^{\text{inc}}$  in the DAR region comes essentially from the ground state ( $\approx 67\%$ ), whereas in the DIF region the forbidden transition are most important. Then it could be interesting to compare the contribution of different multipoles to the folded cross sections for PQRPA vs RQRPA in the DAR and DIF region.

Experimental data on exclusive and other excited states necessary to build the inclusive cross section for antineutrino cases are scarce or null. Figure 4 illustrates the  $\bar{\nu}_e-^{12}\text{C}$  cross sections as a function of the incident antineutrino energy in different nuclear structure models: PQRPA (I) (solid) and (II), CRPA+partial occupations (PO) Ref. [28] and CRPA+PO(nr) non-reduced. Also shown are the cross sections from the uncorrelated factor form (UFF) of Ref. [35] (it is another EPT calculation) and EPT [34]. In the top panel we compare the antineutrino exclusive cross sections,  $\sigma_e^{\text{exc}}$ , where the PQRPA (I) is larger than other ones, if the CRPA+PO(nr) is not taken into account. Below 100 MeV PQRPA (II) is only slightly larger than the other models, and it becomes smaller beyond this energy. In particular, the EFT model is the smallest below 100 MeV, when the other approximations are very close (EFT separates of the group above 55 MeV). This behavior of the EFT antineutrino exclusive cross section of Ref. [34] is different of what is obtained in the neutrino case (see middle panel of Fig. 2) and it could have important consequences for experiments, such as Borexino, LENA and LVD, which use this cross section for the detection of supernovae neu-

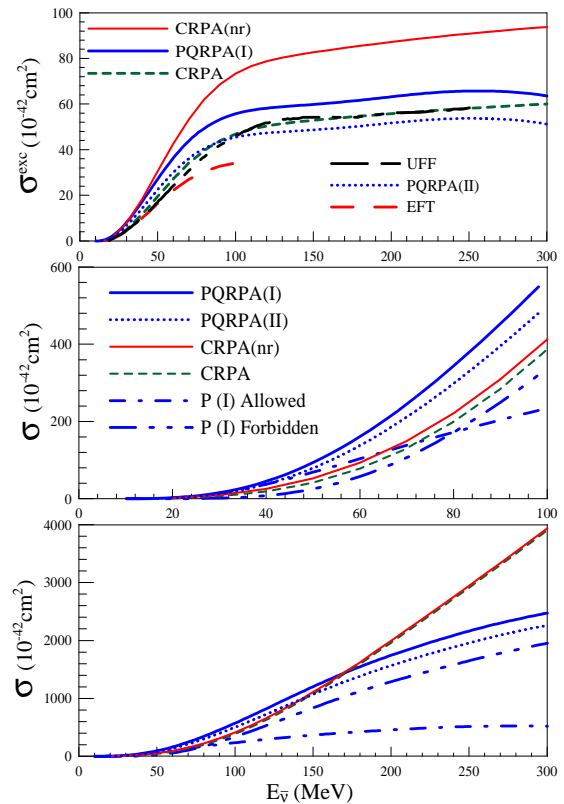


FIG. 4: (Color online)  $\bar{\nu}_e-^{12}\text{C}$  cross sections as a function of the incident antineutrino energy with different nuclear structure models. (top panel) Exclusive cross sections: PQRPA(I) (solid) and (II) (dotted), CRPA plus partial occupations (short dashed) and CRPA(nr) plus partial occupations non-reduced (thin solid) [28], UFF (short-large dashed) [35], EPT (large dashed) [34]. In the middle and bottom panels we compare the inclusive cross sections for PQRPA (I)(solid) and (II) (dotted), CRPA+PO (short dashed) and CRPA+PO(nr) (thin solid) [28] for other neutrino energy interval, as described in the text. For PQRPA (I), we present the allowed (dashed-dot) and forbidden (dashed-dot-dot) contributions.

trinos. The middle panel of Fig. 4 shows  $\sigma_e$  in the energy interval that could be relevant for supernovae neutrinos. In this region the inclusive cross sections show the characteristic increase with  $E_\nu^2$ . The allowed and forbidden contributions for the inclusive cross section are shown for PQRPA (I). We note that below energies of  $\approx 80$  MeV the main contribution to  $\sigma_e^{\text{inc}}$  comes from the AT (showing a change of convexity) and above this value the FT grows faster than the other ones. In the bottom panel of Fig. 4 the mentioned behavior for the forbidden cross sections remains the same through 300 MeV, whereas the allowed cross section begins to saturate at  $\approx 200$  MeV. The forbidden and inclusive PQRPA cross sections still grow slowly and apparently level out beyond 300 MeV. Comparing the  $\sigma_e^{\text{inc}}$  from PQRPA and CRPA (and CRPA(nr)) we note that the PQRPA results are larger than the CRPA's ones below the crossing point at  $\approx 170$  MeV. Above this energy the slope of these cross sections is so different,  $\sigma_e^{\text{inc}}$  of CRPA increases almost

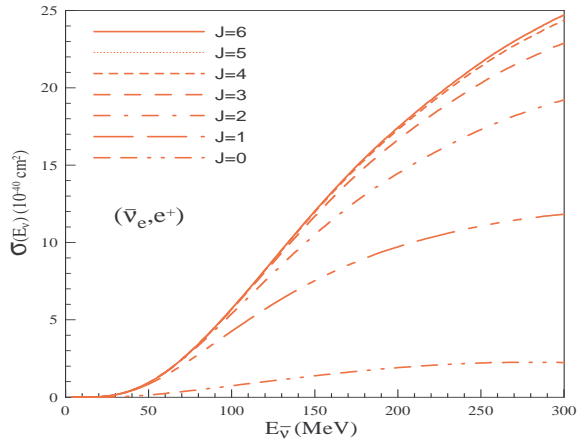


FIG. 5:  $\bar{\nu}_e-^{12}\text{C}$  cross section,  $\sigma(E_{\bar{\nu}})$ , as a function of the  $E_{\bar{\nu}}$  energy in the PQRPA (parametrization P(I)) model for different multipoles showed according to increasing nuclear spin, from  $J_{min} = 0^\pm$  to  $J_{max} = 6^\pm$ .

linearly and  $\sigma_{\bar{e}}^{\text{inc}}$  of PQRPA increases slowly, separating from CRPA. Figure 5 shows the  $\sigma_{\bar{e}}(E_{\bar{\nu}})$  with increasing nuclear spin, according to equation (9). As with the neutrino case, the largest contribution comes from  $J = 1^\pm$  and  $J = 2^\pm$  and the contribution from higher forbiddenness fades out.

To analyze possible observables for the excited multipoles we calculate the folded cross section with the antineutrino fluxes of  $\beta$ -beams in a similar way as was discussed in Ref. [12]. Table II shows the PQRPA (I) and (II) calculated flux-averaged cross section with the partial fraction,

$$\xi_{\ell}(J_f^\pi) = \left[ \frac{\bar{\sigma}_{\ell}(J_f^\pi)}{\bar{\sigma}_{\ell}^{\text{inc}}} \right] \times 100\%, \quad (10)$$

for the  $\nu_e-^{12}\text{C}$  and  $\bar{\nu}_e-^{12}\text{C}$  processes with the conventional electron neutrino and antineutrinos fluxes produced by muon decay-at-rest DAR [19] and those produced by boosted  $^6\text{He}$  ions with  $\gamma = 6$ ,  $\gamma = 10$  and  $\gamma = 14$  adjusting the fluxes of Fig. 4 in Ref. [12] to polynomial forms. From the second and third columns of Table II we note that  $\xi_e(J_f^\pi)$  for  $(\nu_e, e^-)$  reactions with the electron neutrino DAR flux are quasi-identical, *i.e.*, the PQRPA results bring the same fractional contributions for allowed and forbidden transitions (the  $\xi_e(0^+)$  from P(II) are lower than that for P(I) because this multipole is most sensitive to the parameters of the  $ph$  channel). A very similar behavior is shown by  $\xi_{\bar{e}}(J_f^\pi)$  for  $(\nu_e, e^+)$  reactions with the electron antineutrino DAR flux. But in this case the allowed transitions displace a small part of their contribution to the forbidden transitions and the third forbidden appears with  $\xi_{\bar{e}}$  non-zero values. The  $\xi_{\bar{e}}(J_f^\pi)$  for  $(\nu_e, e^+)$  reactions with the electron antineutrino fluxes from  $\beta$ -beam with increasing the boost  $\gamma$  are shown in the last three columns of Table II. According with the increase of  $\gamma$ , the contribution of allowed transitions decrease gradually in favor of the first forbidden

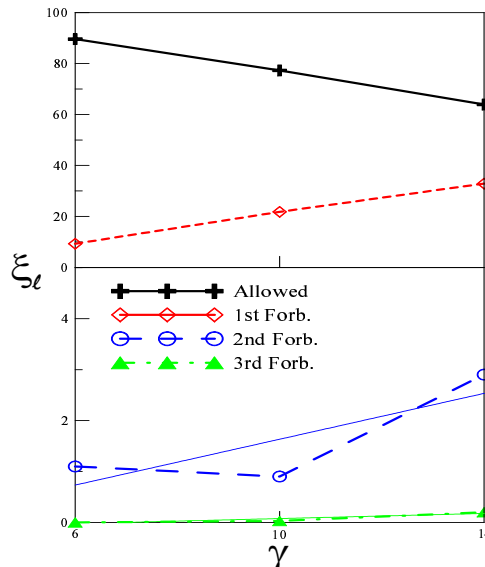


FIG. 6: Partial fraction for calculated flux-averaged antineutrino cross section in  $^{12}\text{C}$  as function of the  $\gamma$ -boost. See text for details.

transition. In particular this is due to the ground state contribution, that brings in average half of contribution to the allowed transition for the different boosts  $\gamma$ . In Fig. 6 we show the evolution of the partial fraction  $\xi_{\bar{e}}$  for allowed, first forbidden (1st forb.), second forbidden (2nd forb.), and third forbidden (3rd forb.), flux-averaged antineutrino cross section in  $^{12}\text{C}$  as a function of the  $\gamma$ -boost. The decreasing slope in the allowed transitions changes to an increasing slope of the forbidden transition, amounting to 92 %, 7 % and 1 % for the 1st forb., 2nd forb. and 3rd forb. transitions, respectively.

#### IV. SUMMARIZING CONCLUSIONS

The  $\nu_e-^{12}\text{C}$  cross sections calculated in the PQRPA model are compared with those evaluated in similar RPA-like models. The exclusive,  $\sigma_{\bar{e}}^{\text{exc}}(E_{\nu})$ , and inclusive,  $\sigma_{\bar{e}}^{\text{inc}}(E_{\nu})$ , antineutrino cross sections are evaluated for the first time in the PQRPA model. Theoretical uncertainties of  $\approx 20\%$  are seen for the cross sections with the weak observables in the  $\{^{12}\text{B}, ^{12}\text{C}, ^{12}\text{N}\}$  triad. Ref. [59] states that it does not matter which nuclear model is used to evaluate  $\sigma_{\bar{e}}^{\text{exc}}(E_{\nu})$ , as long as the constrains such as the positron decay of  $^{12}\text{N}$ , the  $\beta$ -decay of  $^{12}\text{B}$ , the M1 strength of the 15.11 MeV state in  $^{12}\text{C}$ , and the partial muon capture rate leading the ground state of  $^{12}\text{B}$  are obeyed. The major of these constrains (we do not evaluate the M1 strength) and additional data on other partial muon capture rates are taken into account in the PQRPA as it is shown in Table I. Nevertheless, the behavior of exclusive cross section for electron antineutrino as a function of energy is not so similar as in the neutrino case. The EFT model seems to move away from the other models. This could be due to the need to describe

TABLE II: Calculated flux-averaged cross section in partial fraction,  $\xi(J_f^\pi)$ , for the  $^{12}\text{C}(\nu_e, e^-)^{12}\text{N}$  process with the conventional neutrino source for the decay-at-rest of muons (DAR) and  $^{12}\text{C}(\bar{\nu}_e, e^+)^{12}\text{B}$  reactions with the anti-neutrino fluxes DAR and those produced by boosted  $^6\text{He}$  ions with  $\gamma = 6$ ,  $\gamma = 10$  and  $\gamma = 14$ .

$\xi(J_f^\pi)$	$(\nu_e, e^-)$		$(\bar{\nu}_e, e^+)$					
	P(I)	P(II)	P(II)	P(I)	P(I)			
	DAR		DAR		$\gamma = 6$	$\gamma = 10$	$\gamma = 14$	
Allowed	82.6	83.0	79.9	79.9	89.6	77.3	63.9	
$1_1^+$	45.9	43.4	35.9	36.4	59.5	34.8	23.8	
$0^+$	8.9	7.3	11.2	13.1	8.6	13.0	13.4	
$1^+$	73.7	75.7	68.7	66.8	81.0	64.2	50.5	
First forbidden	16.9	16.6	19.6	19.6	9.3	21.8	32.9	
$0^-$	0.3	0.4	0.7	0.6	0.4	0.7	0.7	
$1^-$	8.9	8.5	11.9	12.3	5.5	13.9	22.0	
$2^-$	7.7	7.7	7.0	6.6	3.4	7.2	10.2	
Second forbidden	0.4	0.4	0.5	0.5	1.1	0.9	2.9	
$2^+$	0.3	0.3	0.3	0.3	0.8	0.6	1.8	
$3^+$	0.1	0.1	0.2	0.2	0.3	0.3	1.1	
Third forbidden	0.0	0.0	0.02	0.02	0.0	0.03	0.2	
Forth forbidden	0.0	0.0	0.0	0.0	0.0	$4 \times 10^{-4}$	0.01	

several bound states in  $^{12}\text{B}$ , whereas in  $^{12}\text{N}$  it is only the ground state that matters, and the EFT description avoids the use of the nuclear wave functions, that the other models employ. This is an important issue to be clarified because future experiments are using EFT models to estimate events on supernovae neutrino [23, 57, 58].

An explicit comparison of the contribution of the different multiplicities to  $\sigma_e^{\text{inc}}(E_\nu)$  in the PQRPA is shown with recent results in the RQRPA [31]. The contribution of these multipoles to the inclusive cross section are shown to be similar in both models, the main contribution comes from the allowed and first forbidden, and to a smaller amount from the second forbidden, *i.e.*, the contribution from the higher forbiddenness decreases in a gradual manner. This characteristic behavior is also displayed by the antineutrino cross sections.

The different behavior of the  $\sigma_{e,\mu}^{\text{inc}}(E_\nu)$  from RPA,

PQRPA, RQRPA and SM with the CRPA and LFG+RPA (it is also shown for the  $\sigma_e^{\text{inc}}(E_\nu)$ ) in the MeV to GeV neutrino energy range claims detailed experimental and theoretical studies [44]. As the main effects are present in the forbidden transitions, we present the partial fraction in percentage to the inclusive flux-averaged antineutrino cross section with the antineutrino fluxes of  $\beta$ -beams. In the  $\bar{\nu}_e-^{12}\text{C}$  reaction we note that according with the increase of  $\gamma$ -boosts, the contribution of allowed transitions decreases gradually in favor of the first forbidden transitions. These results enhances the feasibility of  $\beta$ -beams to study nuclear response in low-energy neutrino region.

This work was partially supported by the U.S. DOE grants DE-FG02-08ER41533 and DE-FC02-07ER41457 (UNEDF, SciDAC-2).

- 
- [1] C. Athanassopoulos *et al.* [LSND Collaboration], Phys. Rev. C **54**, 2685 (1996); Phys. Rev. Lett. **77**, 3082 (1996).  
[2] C. Athanassopoulos *et al.* [LSND Collaboration], Phys. Rev. C **58**, 2489 (1998); Phys. Rev. Lett. **81**, 1774 (1998).  
[3] A. Aguilar *et al.* [LSND collaboration], Phys. Rev. D **64**, 112007 (2001).  
[4] Y. Fukuda *et al.* [Super-Kamiokande Collaboration], Phys. Rev. Lett. **81**, 1562 (1998); Y. Ashie *et al.* [Super-Kamiokande Collaboration], Phys. Rev. Lett. **93**, 101801 (2004).  
[5] B. Aharmim *et al.* [SNO Collaboration], Phys. Rev. C **59**, 055502 (2005); M. B. Smy *et al.* [Super-Kamiokande Collaboration], Phys. Rev. D **69**, 011104 (2004).  
[6] T. Araki *et al.* [KamLAND Collaboration], Phys. Rev. Lett. **94**, 081801 (2005).  
[7] M. H. Ahn *et al.* [K2K Collaboration], Phys. Rev. Lett. **90**, 041801 (2003).  
[8] A. Fassler *et al.*, arXiv:0711.3996v2[nucl-th], to be apper in J. Phys. G: Nucl Phys.(2008).  
[9] G. McLaughlin and G. M. Fuller, Astrop. J. **455**, 202 (1995).  
[10] A. B. Balantekin, J. Phys.: Conf. Ser. **49**, 99 (2006).  
[11] Y.-Z. Qian and J. Wassweburg, Phys. Rep. **442**, 237 (2007).  
[12] R. Lazauskas and C. Volpe, Nucl. Phys. **A792**, 219 (2007).  
[13] J.S. O'Connell, T.W. Donnelly and J.D. Walecka, Phys. Rev. **6**, 719 (1972).  
[14] T.W. Donnelly and W.C. Haxton, Atomic Data and Nuclear Data Tables **23**, 103 (1979); T. W. Donnelly and R. D. Peccei, Phys. Rep. **50**, 1 (1979).  
[15] T. Kuramoto, M. Fukugita, Y. Kohyama and K. Kubodera, Nucl. Phys. **A512**, 711 (1990).  
[16] J. R. Luyten, H. P. C. Rood and H. A. Tolhoek,

- Nucl.Phys. **41**,236 (1963).
- [17] F. Krmpotić, A. Mariano and A. Samana, Phys. Rev. C **71**, 044319 (2005).
- [18] R. Maschuw *et al.* KARMEN Collaboration, Prog. Part. Phys. **40**, (1998) 183; and references therein mentioned.
- [19] B. Armbruster *et al.*, KARMEN collaboration, Phys. Rev. D **65**, 112001 (2002).
- [20] R. C. Allen *et al.*, Phys. Rev. Lett. **64**, 1871 (1990).
- [21] D. A. Krakauer *et al.*, Phys. Rev. C **45**, 2450 (1992).
- [22] Y. Efremenko, Nucl. Phys. **B138**(Proc. Suppl), 343 (2005); F.T. Avignone III and Y.V. Efremenko, J. Phys. G **29**,2615 (2003).
- [23] N.Yu. Agafonova *et al.*, Astron. Phys. **27**, 254 (2007).
- [24] C. Volpe, N. Auerbach, G. Colò, T. Suzuki, N. Van Giai, Phys. Rev. C **62**, 015501 (2000).
- [25] N. Auerbach, N. Van Giai, and O. K. Vorov, Phys. Rev. C **56**, 2368 (1997).
- [26] S. K. Singh, N. C. Mukhopadhyay, and R. Oset, Phys. Rev. C **57**, 2687 (1998).
- [27] E. Kolbe, K. Langanke and S. Krewald, Phys. Rev. C **49**, 1122 (1994).
- [28] E. Kolbe, K. Langanke and P. Vogel Nucl. Phys. **A652**, 91 (1999).
- [29] N. Jachowicz, S. Rombouts, K. Heyde, and J. Ryckebusch, Phys. Rev. C **59**, 3246 (1999); N. Jachowicz, K. Heyde, J. Ryckebusch, and S. Rombouts, Phys. Rev. C **65**, 025501 (2002).
- [30] A. Samana, F. Krmpotić, A. Mariano and R. Zukanovich Funchal, Phys. Lett. **B642**, 100 (2006).
- [31] N. Paar, D. Vretenar, T. Marketin and P. Ring, Phys. Rev. C **77**, 024608 (2008).
- [32] J. Nieves, J.E. Amaro, and M. Valverde Phys. Rev. C **70**, 055503 (2004).
- [33] M. Valverde, J.E. Amaro, and J. Nieves Phys. Lett. **B638**, 325 (2006).
- [34] M. Fukugita, Y. Kohyama and K. Kubodera, Phys. Lett. **B212**, 139 (1988).
- [35] S.L. Mintz, Phys. Rev. C **25**, 1671 (1982); S.L. Mintz and M. Pourkaviani, J. Phys. G **15**, 1241 (1989); *ibid*, Phys. Rev. C **40**, 2458 (1989).
- [36] S.L. Mintz and M. Pourkaviani, J. Phys. G **20**, 925 (1994); *ibid* Nucl. Phys. **A594**, 346 (1995).
- [37] M.S. Athar, A. Ahmad and S.K. Singh, Nucl. Phys. **A764**, 551 (2006).
- [38] A.C. Hayes and I.S. Towner, Phys. Rev. C **61**, 044603 (2000).
- [39] N. Auerbach and B.A. Brown, Phys. Rev. C **65**, 024322 (2002).
- [40] F. Krmpotić, A. Mariano and A. Samana, Phys.Lett. **B541**, 298 (2002).
- [41] A.R. Samana and C.A. Bertulani, <http://arxiv.org/abs/0802.1553v2>, Phys. Rev. C, in press.
- [42] F. Krmpotić, A. Mariano, T.T.S. Kuo, and K. Nakayama, Phys. Lett. **B319**, 393 (1993).
- [43] E. Kolbe, K. Langanke and G. Martínez-Pinedo, Phys. Rev. C **60**, 052801 (1999).
- [44] J. Serreau and C. Volpe, Phys. Rev. C **70**, 055502 (2004).
- [45] J. Hirsch and F. Krmpotić, Phys. Rev. C **41**, 792 (1990).
- [46] J. Hirsch and F. Krmpotić, Phys. Lett. **B246**, 5 (1990).
- [47] F. Krmpotić, J. Hirsch and H. Dias, Nucl. Phys. **A542**, 85 (1992).
- [48] F. Krmpotić and Shelly Sharma, Nucl. Phys. **A572**, 329 (1994).
- [49] G. H. Miller *et al.*, Phys. Lett. B **41**, 50 (1972).
- [50] D.F. Measday, Phys. Rep. **354**, 243 (2001).
- [51] T.J. Stocki, D.F. Measday, E. Gete, M.A. Saliba, and T.P. Gorringe, Nucl. Phys. **A697**, 55 (2002).
- [52] T. Suzuki, D.F. Measday, and J.P. Roalsvig, Phys. Rev. C **35**, 2212 (1987).
- [53] L-B. Auerbach *et al.* [LSND Collaboration], Phys. Rev. C **64**, 065501 (2001); C. Athanassopoulos *et al.* [LSND Collaboration], Phys. Rev. C **55**, 2078 (1997).
- [54] L-B. Auerbach *et al.* [LSND Collaboration], Phys. Rev. C **66**, 015501 (2002).
- [55] F. Ajzenberg-Selove, Nucl. Phys. **A433**, 1 (1985); TUNL Nuclear Data Evaluation Project, available WWW: <http://www.tunl.duke.edu/nucldata/>
- [56] D. E. Alburger and A.M. Nathan, *Phys. Rev. C* **17** (1978) 280.
- [57] L. Cadonati, F. P. Calaprice and M. C. Chen, Astrop. Phys. **16**, 361 (2002).
- [58] T. Marrodán Undagoitia *et al.*, Prog. Part. Nucl. Phys. **57**, 283 (2006)
- [59] E. Kolbe, K. Langanke, G. Martínez Pinedo and P. Vogel, J. Phys. G **29**, 2569 (2003).